ACS OMEGA

Open Access

http://pubs.acs.org/journal/acsodf

Article

Insights in Electrochemical Determination of Quercetin in Peach Vinegar by the Hexagonal Platinum Nanocrystal

Ying Zhang, Xilin Peng,* and Feng Gao*

Cite This: *ACS Omega* 2024, 9, 1850−1857

Read Online

ACCESS | Metrics & More | Article Recommendations | Supporting Information

ABSTRACT: Peach vinegar is a popular condiment that is thought to have various health benefits. However, the low levels of quercetin and complex detection environment in peach vinegar make it difficult to detect using traditional methods. Electrochemical detection is a promising solution because it is sensitive, inexpensive, and provides real-time results. Herein, a hexagonal Pt nanocrystal was developed as an electrocatalyst for selective detection of quercetin in peach vinegar, and a comprehensive examination was given of the electrochemical characteristics of quercetin when applied to electrodes modified with platinum. The morphology and crystal properties of Pt nanocrystals were analyzed, and the Pt-modified electrode was found to exhibit strong electrocatalytic effects toward quercetin in peach vinegar with a high sensitivity of 58 μA μM^{-1}. Furthermore, the investigation showcased exceptional specificity, consistency, sustained durability, and replicability of the Pt-modified electrode in identifying quercetin. The detection result of the Pt-modified electrode tested in three different peach vinegar samples demonstrated its practical utility in real-world applications. Overall, the findings of this study may have important implications for the development of more efficient and sensitive electrochemical sensors for the detection of quercetin and other analytes in vinegar.

1. INTRODUCTION

In recent years, food safety and quality have become significant concerns for consumers worldwide. Vinegar is a widely used condiment that is believed to offer various health benefits.[1−3] However, it can also be contaminated with harmful substances, such as heavy metals, or adulterated with cheaper substitutes. To address these issues, researchers have been exploring the use of various methods for selective detection of specific compounds in vinegar.[4,5] In particular, the detection of quercetin, a flavonoid found in many fruits and vegetables known for its antioxidant properties, has gained attention due to its potential health benefits. For example, quercetin has shown promising anticancer activity, inhibiting and preventing various types of cancers such as breast, lung, and colon cancer, and plays a role in cardiovascular health by lowering cholesterol levels and preventing the formation of arterial plaque, thus reducing the risk of heart disease.[6−8] However, the investigation was neglected in peach vinegars. Generally, the content of quercetin in peach vinegar is a trace amount; thus, numerous difficulties have been brought to the detection of quercetin with traditional methods, including fluorescence,[9] spectrophotometry,[10,11] and capillary electrophoresis,[12,13] due to their high cost, low sensitivity, and poor real-time response properties. Hence, the pursuit of novel approaches to achieve the precise identification of quercetin continues to pose a significant obstacle.

The electrochemical detection method has emerged as a promising means to identify specific constituents in solutions, owing to its heightened sensitivity, instantaneous feedback, and cost-effectiveness.[14−16] Through an effective chemical reaction on the surface of the electrocatalyst, a microcurrent can be formed, and the trace component can be detected by an amplification of the current signal. However, there are some challenges that must be addressed. One of the main problems is interference from other compounds present in peach vinegar. Because vinegar is a complex matrix that contains a variety of organic acids, sugars, and polyphenols, it can be difficult to differentiate quercetin from other compounds that have similar electrochemical properties. This can lead to false positive or negative results, which affect the accuracy and reliability of the analysis. Another challenge is the lack of suitable electrode materials for quercetin detection in peach vinegar. Traditional electrode materials, such as glassy carbon and carbon nanotubes, may not be effective for detecting quercetin due to their limited selectivity and sensitivity. Therefore, new electrode materials with high selectivity toward quercetin need to be developed for accurate detection.

Electrocatalysts play an important role in electrochemical detection by accelerating electrochemical reactions and increasing the sensitivity and selectivity of electrochemical detection.[17−19] Recently, several electrocatalysts have been reported for the detection of quercetin, including multiwalled carbon nanotubes,[20] Co_3O_4,[21] and graphene-based composite.[22−24] However, there are several limitations to consider. Carbon nanomaterials, like carbon nanotubes and carbon quantum dots, offer a large surface area and impressive electrochemical properties, but their complex synthesis process

Received: October 28, 2023
Revised: November 28, 2023
Accepted: December 13, 2023
Published: December 28, 2023

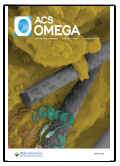

Scheme 1. Representation Showcasing the Steps Involved in Preparing and Utilizing Pt/GCE

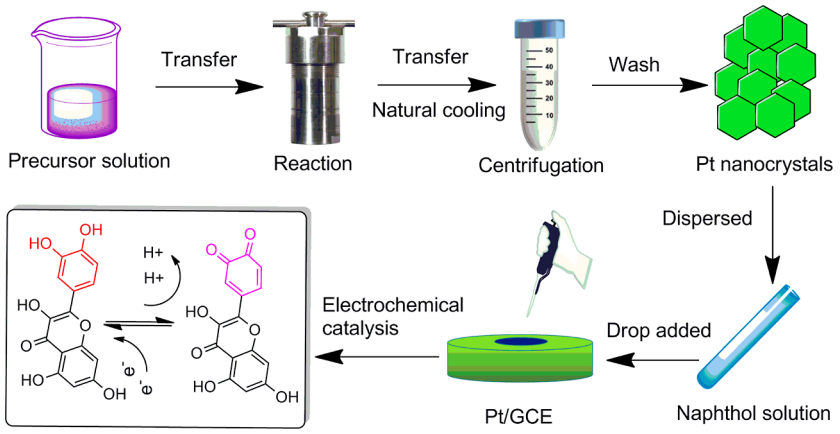

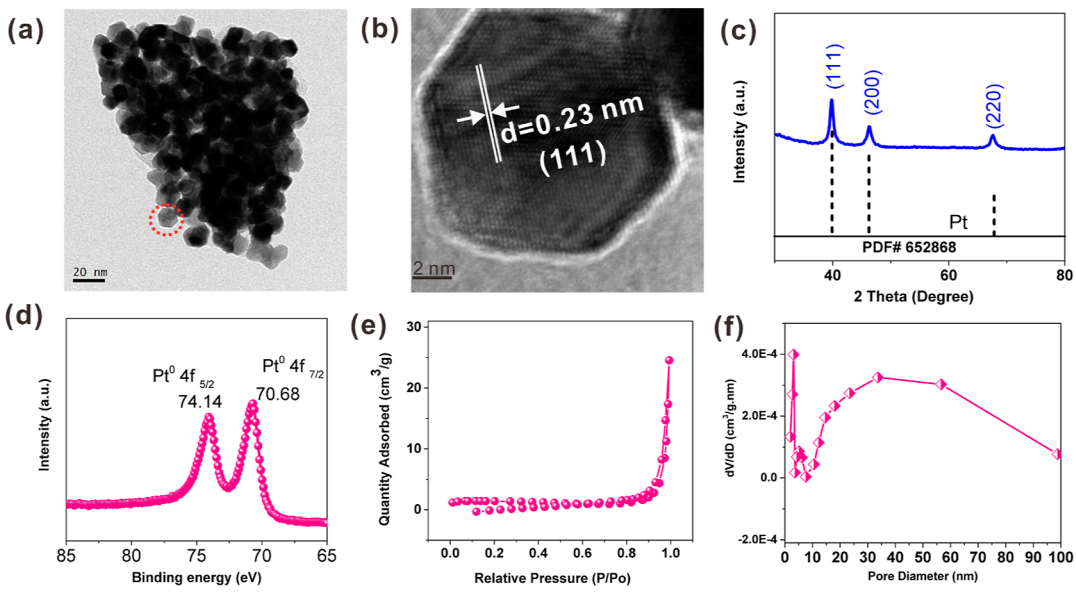

Figure 1. (a) TEM, (b) HRTEM, and (c) XRD measurements of Pt nanocrystals; (d) XPS spectrum of Pt 4f region; (e) N_2 adsorption–desorption isotherms of Pt nanocrystals; and (f) corresponding differential distribution pattern of particle size versus volume.

constraints hinder their widespread use. Metal oxide nanoparticles have good electrochemical catalytic activity and surface-enhanced effects, which can improve detection sensitivity. However, aggregation phenomena may occur during long-term use, leading to signal attenuation or instability issues. Based on the aforementioned limitations, developing catalysts with high stability and excellent detection performance is indeed necessary.

Platinum (Pt) is a well-known electrocatalyst that has been widely used in various electrochemical systems, including electrochemical detection.[25−28] It has excellent catalytic activity toward many analytes and is compatible with a wide range of solvents, which allows for accurate and sensitive detection even at low concentrations.[19,29,30] Besides, Pt-based electrodes have a long lifespan compared with other electrocatalysts, reducing the need for frequent replacement or maintenance.

As far as we know, there have been no previous studies on the specific electrochemical detection of quercetin in peach vinegar. This is primarily due to the challenges posed by the low quercetin content and complex composition of the vinegar. In order to achieve precise detection of quercetin content in peach vinegar and enable trace analysis, we synthesized hexagonal Pt nanocrystals as the electrocatalyst to investigate the specific influence of crystal morphology and surface conditions on catalyzing quercetin in the complex environment of peach vinegar. This hexagonal sheetlike structure provides large planar active sites for redox reactions and increases the binding area between a single crystal and naphthol, which effectively reduces the detachment of Pt nanocrystals from the electrode surface. As a result, the electrode achieved excellent detection performance for quercetin in peach vinegars, with a limit of detection (LOD) as low as 1.4 nM.

2. EXPERIMENTAL SECTIONS

2.1. Reagents and Sources. All the chemicals, such as H_2PtCl_6 (AR), KOH (AR), ethylene glycol (AR), naphthol (5% in ethanol), *N*,*N*-dimethylacetamide (DMF) (AR), H_3PO_4 (85%, AR), CH_3COOH, and H_3BO_3, were obtained from Shanghai McLean Biochemical Technology Co., Ltd.

2.2. Synthesis of Pt Nanocrystals. To form a uniform solution, 2 g of potassium hydroxide was dissolved in a mixture of 10 mL of ethylene glycol and 50 mL of DMF. Next, 1 mL of chloroplatinic acid solution with a concentration of 0.1 g/mL

https://doi.org/10.1021/acsomega.3c08513
ACS Omega 2024, 9, 1850−1857

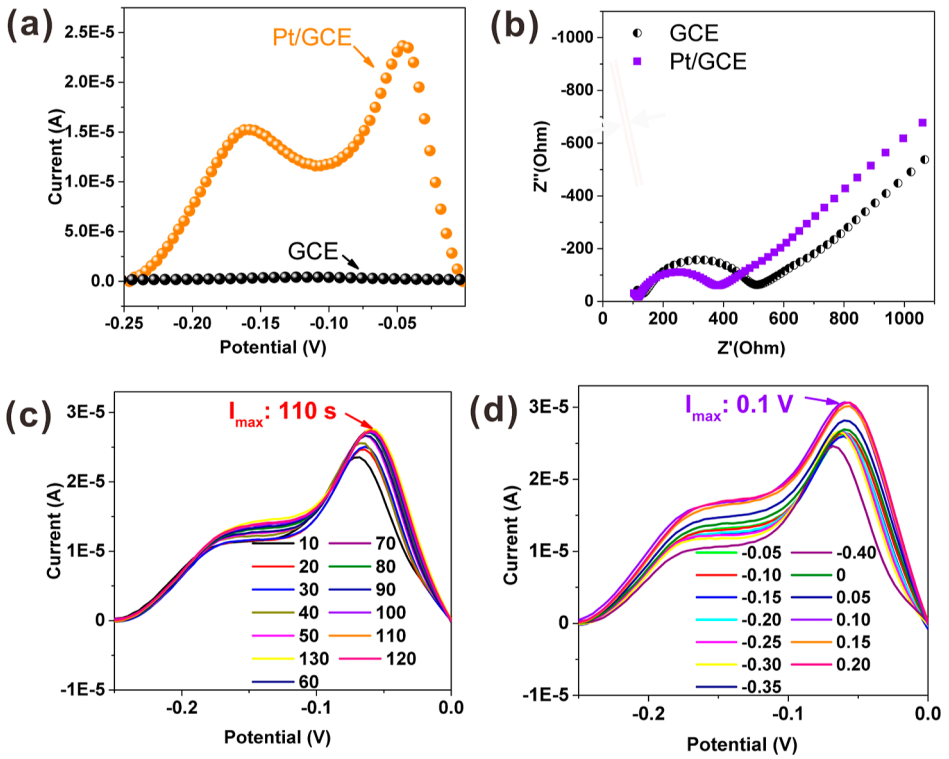

Figure 2. DPV data obtained by immersing electrodes in a Britton−Robinson solution (pH 2.0) with a concentration of 100 nM quercetin. (b) EIS spectra. (c) DPV responses showing the effect of accumulation time, with an accumulation potential of 0.35 V. (d) DPV responses displaying the impact of varying accumulation potentials while keeping the accumulation time fixed at 110 s.

was added to the mixture and stirred for 2 h to create a precursor solution. The precursor solution was placed in a Teflon-lined reaction vessel and subjected to a reaction at 160 °C for a duration of 8 h. After cooling naturally, the reacted solution was centrifuged to gather a black precipitate, which was thoroughly rinsed with ethanol, repeating the process at least three times. Finally, the Pt nanocrystals were obtained by drying the black precipitate at 60 °C for 12 h.

2.3. Preparation of the Pt/GCE Modified Electrode. A uniform dispersion was prepared by dispersing 1 mg of Pt nanocrystal in 1 mL of naphthol solution (0.5%) for use. The GCE underwent a polishing process using Al_2O_3 powder of 0.5 and 0.3 mm sizes consecutively. Subsequently, it was subjected to ultrasonic cleaning in deionized water for a duration of 5 min. A 5 μL solution was carefully applied to the upper surface of the GCE and allowed to air-dry naturally, resulting in the creation of a Pt-modified electrode (Pt/GCE). The schematic representation of the procedure for modifying the GCE electrode with Pt nanocrystals is illustrated in Scheme 1.

2.4. Methods and Measurements. This part can be found in the Supporting Information. Please refer to "1.1 Methods and measurements" in the Supporting Information for experimental detail.

3. RESULTS AND DISCUSSION

3.1. Characterization of Pt Nanocrystals. The morphology of the Pt nanocrystals produced was measured, and as shown in Figure 1a, the nanocrystals had a uniform hexagonal slice shape with an average size of 8−10 nm (Figure S1, Supporting Information). To further examine the crystal structure, we amplified the region marked with a red circle in Figure 1a and obtained the high-resolution transmission electron microscopy (HRTEM) image shown in Figure 1b, which exhibited a distance between adjacent planes of 0.23 nm, aligning closely with the lattice plane denoted as (111).[31] We also recorded the X-ray diffraction (XRD) pattern of the Pt nanocrystals to verify their crystal structure. The diffraction signals observed at angles of 39.8, 46.2, and 67.6° could be assigned to the (111), (200), and (220) planes of Pt crystal, respectively, and were consistent with the standard card (PDF# 65-2868). Additionally, we measured the high-resolution X-ray photoelectron spectroscopy (XPS) spectrum of Pt 4f, and as illustrated in Figure 1d, two peaks appeared at 70.68 and 74.14 eV, corresponding to the Pt° $4f_{7/2}$ and Pt° $4f_{5/2}$ orbitals, respectively,[25] confirming the reduction of Pt element in chloroplatinic acid to zerovalent metal Pt. Finally, we evaluated the surface area of the Pt nanocrystals using N_2 adsorption−desorption isotherm measurement (Figure 1e), and the Brunauer−Emmett−Teller surface area was estimated to be 4.5 $m^2\ g^{-1}$. Besides, the particle size distribution has been investigated by the differential distribution pattern of particle size versus volume, where the particle size mainly lies in the region of 5−10 nm, which agrees well with the TEM result (Figure 1f).

3.2. Electrochemical Analysis of Electrodes toward Quercetin. We investigated the electrochemical analytical effect of quercetin on the GCE and Pt/GCE electrodes by analyzing their differential pulse voltammetry (DPV) response curves. As depicted in Figure 2a, the bare GCE electrode did not display any catalytic effect toward quercetin due to insignificant redox signals. However, the Pt-modified GCE electrode produced two distinct redox signals located at −0.046 and −0.161 V, indicating the strong reaction of quercetin involves the participation of two-proton and double-electrodes, which occurs step by step, with each gain or loss of

https://doi.org/10.1021/acsomega.3c08513
ACS Omega 2024, 9, 1850−1857

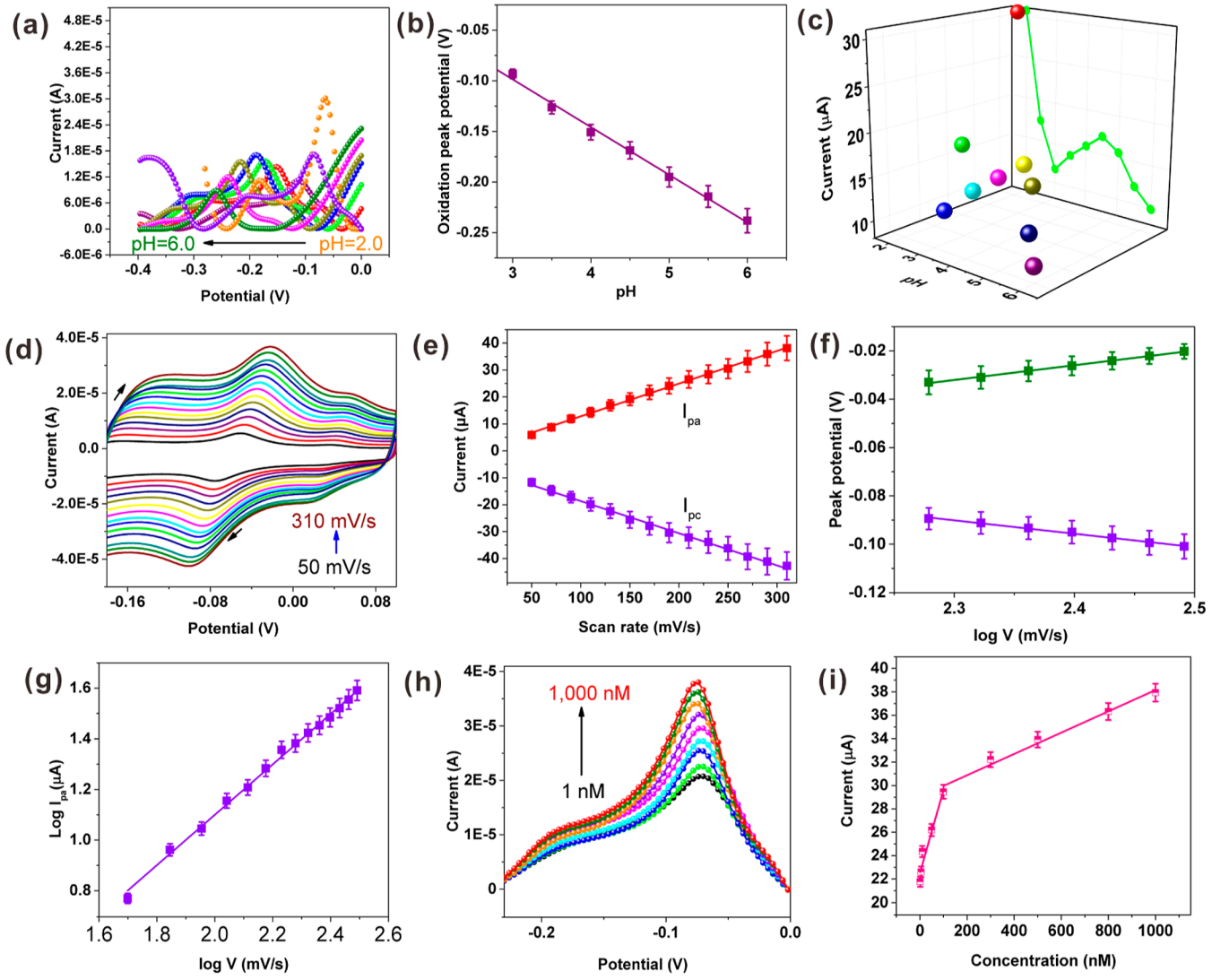

Figure 3. (a) DPV response (100 nM quercetin); (b) oxidation peak potential and (c) oxidation peak current versus pH values; (d) CV curves at different scan rates (the interval: 20 mV s^{-1}) in Britton−Robinson solution; (e) corresponding dependence of peak currents on the scan rate; (f) dependence of peak potential on log ν; (g) linear fitting of log I_{pa} versus log ν. (h) DPV responses (quercetin concentration ranging from 1 to 1000 nM); and (i) correlation between the maximum current and the concentration of quercetin using a linear regression model.

an electron/proton corresponding to an electrochemical signal. This result is in good agreement with the CV curves (Figure S2, Supporting Information). Additionally, we studied the impedance properties of the Pt/GCE electrode through an electrochemical impedance spectroscopy measurement (EIS). The semicircle value of the high-frequency region represents the reverse reflection of the electron-transfer resistance (R_{ct}).[32] As illustrated in Figure 2b, the R_{ct} values for the bare GCE were estimated to be 510 Ω, but they decreased significantly after decorating with Pt nanocrystals, demonstrating that the electrochemical electron transfer process could be facilitated effectively in the Pt/GCE electrode.

3.3. Accumulation Time and Potential. We examined the influence of accumulation time and potential affecting the DPV output when using a Pt/GCE for detecting quercetin (100 nM) (Figures 2c,d and S3−S4, Supporting Information). As the accumulation time increased, the peak current of the DPV output initially rose before showing a slight decline and eventually reaching its highest value at an accumulation duration of 110 s. Likewise, at an accumulation potential of 0.1 V, we observed the highest peak current. Taking these outcomes into account, we determined that an accumulation time of 110 s and a potential of 0.1 V were optimal for future experiments.

3.4. pH Effect. The pH value is a key factor influencing the electrochemical reaction.[23,33] We investigated the impact of pH on DPV responses for 100 nM quercetin in Britton−Robinson solutions (Figure 3a). We examined the relationship between pH and peak current to determine their correlation. As illustrated in Figure 3b, the connection between oxidation peak current (E_{ox}) and pH can be accurately described by an equation: E_{ox}−0.054 pH + 0.044 (R^2 = 0.9958). The −0.054 slope value exhibited by this equation demonstrates a remarkable proximity to the theoretical value of −0.059, thereby implying that the redox reaction entails an equal involvement of electrons and protons.[33] Besides, the impact of pH on the oxidation peak current was studied (Figure 3c). The pH value of 2.0 yields the highest peak current, and thus it is selected for subsequent experiments.

https://doi.org/10.1021/acsomega.3c08513
ACS Omega 2024, 9, 1850−1857

Table 1. Evaluation of the Effectiveness of Various Electrodes for Detecting Quercetin

electrode	linear range (μM)	LOD (nM)	sensitivity (μA μM^{-1})	ref
PB-rGO/TCD/AuNPs/GCE	0.005−0.4	1.83	36.19	23
Pd/MoS_2−IL-OMC/GCE	0.02−10	8	10.6	35
Co_3O_4/GCE	0.01−3	0.2	2.99	21
Pt-PDA@SiO_2/GCE	0.05−0.383	16	6.47	30
p[DqCrC]@Co-NC	0.01−21.4, 1.4−150	14		36
AgNPs@g-CN	0.01−120	6	0.0351	37
CD/AuNPs/MWCNTs/GCE	0.005−7	6.4	4.701	38
SeO2/rGO/GCE	0.01−200	1.6	50	39
Pt/GCE	0.001−0.1, 0.1−1.0	1.4	58	this work

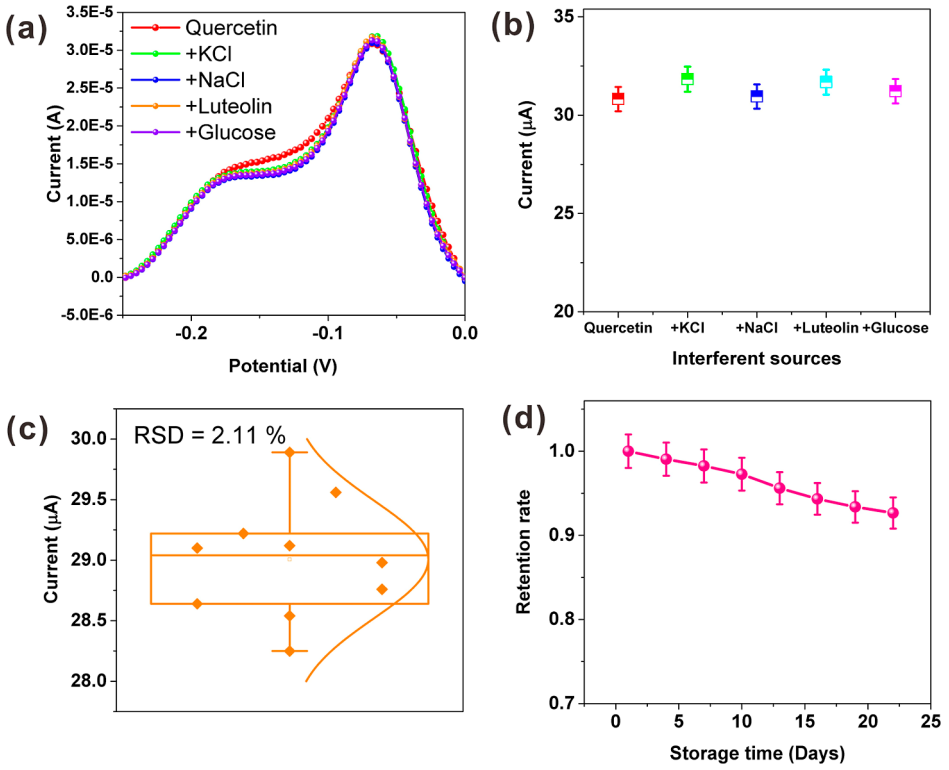

Figure 4. (a) Influences of equal molar concentrations of common ions and media coexisted; (b) corresponding peak current; (c) statistic of the peak current of DPV responses of the Pt/GCE electrode toward quercetin from ten repeat measurements; and (d) peak current retention rate.

3.5. Electrochemical Behavior. The CV profiles were examined at various scan rates (v). As shown by Figure 3d, The cyclic voltammetry plots of the Pt/GCE electrode toward quercetin exhibit a set of redox peaks that demonstrate reversibility. Furthermore, the peak current shows an upward trend as the scanning rate increases. The relationship between the redox peak current and the scan rate obeys two good linear fitting equations (Figure 3e): I_{pa} (uA) = 0.118v + 0.65 (R^2 = 0.9973) and I_{pc} (uA) = −0.118v + 0.63 (R^2 = 0.9944), where I_{pa}, I_{pc}, and v represent the anodic peak current, cathodic peak current, and scan rate, respectively. The direct proportionalities observed between the peak current and scan rate provide evidence that the adsorption process governs the redox reaction in solution.[22]

We examined the association between the logarithm of v and maximum potentials to explore the determination of electron transfer number (n) and electron transfer coefficient (α). As displayed in Figure 3f, the peak potential versus log v meets with linear equations: E_{pa} (V) = 0.059 log v (mV/s) − 0.19 (R^2 = 0.9982) and E_{pc} (V) = −0.056 log v (mV/s) + 0.035 (R^2 = 0.9932), where E_{pa} and E_{pc} represent the anodic and cathodic peak potential, respectively. In theory, the relationship between the maximum potential and the logarithm of v is expected to conform to the two Laviron equations[24]

$$E_{pa}(V) = E^0 + \frac{2.303RT}{(1-\alpha)nF}\log v + \frac{2.303RT}{(1-\alpha)nF}\log\frac{nF(1-\alpha)}{RTK_s} \quad (1)$$

$$E_{pc}(V) = E^0 - \frac{2.303RT}{\alpha nF}\log v - \frac{2.303RT}{\alpha nF}\log\frac{\alpha nF}{RTK_s} \quad (2)$$

within the given context, E^0 denotes the standard redox potential, R signifies the universal gas constant, T represents the absolute temperature measured in Kelvin, F symbolizes the Faraday constant (96,485 C mol^{-1}), and K_s stands for the rate constant pertaining to heterogeneous electron transfer. The calculated ratio of slopes $\alpha/(1-\alpha)$ for the two equations is 1.05, which leads to an α value of 0.51. Taking the α value into eqs 1 or (2), we can gain an n value of 2.04. The

https://doi.org/10.1021/acsomega.3c08513
ACS Omega 2024, 9, 1850−1857

aforementioned outcome provides evidence that an equal quantity of protons and electrons participate in the redox mechanism. Consequently, it can be inferred without difficulty that the redox process involves the involvement of two electrons and twice the number of protons. We further investigated the relationship between log I_{pa} and scan rate log v. As illustrated in Figure 3g, the correlation can be represented by a linear regression equation: log I_{pa} (uA) = 0.97 log v − 0.76 (R^2 = 0.9972). The slope value of 0.97, which is near the theoretical adsorption control value of 1.0, provides confirmation that the redox reaction of quercetin on the Pt/GCE electrode is effectively regulated by the process of adsorption.

Theoretically, the reaction kinetics process is concentration dependent.[34] In order to gain a better understanding of the connection between the DPV response and the concentration of quercetin, we examined the DPV response of quercetin on the Pt/GCE electrode in a Britton−Robinson solution, employing various concentrations of quercetin. As depicted in Figure 3h, the current of the oxidation peak exhibits a gradual increment as the concentration of quercetin rises. The association between the oxidation peak current and the concentration of quercetin adheres to two separate linear models (Figure 3i), where the linear equations are I_{pa} (uA) = 0.058 C (nM) + 24.69 (R^2 = 0.9976 and 1 nM ≤ C ≤ 100 nM) and I_{pa} (uA) = 0.00088 C (nM) + 30.64 (R^2 = 0.9985, 100 nM ≤ C ≤ 1000 nM). The Pt/GCE electrode exhibits an impressive sensitivity of 58 μA μM^{-1} toward quercetin. Based on the formula that LOD equals 3 times the standard deviations divided by the sensitivity (S), the estimated LOD is 1.4 nM. Our findings surpass the majority of prior studies (refer to Table 1).

3.6. Selectivity, Stability, Repeatability, and Reproducibility Analysis. To examine the selectivity of the Pt/GCE electrode, we investigated the impacts of common ions and media such as K^+, Na^+, Cl, luteolin, and glucose on quercetin detection (Figure 4a). The subtle rise or fall in the DPV oxidation peak current across all specimens highlights the Pt/GCE electrode's remarkable resistance to interference under intricate detection circumstances (Figure 4b). The detection repeatability was measured by performing ten parallel experiments. As shown in Figure 4c, a low related standard deviation (RSD) of 2.11% was achieved for the Pt/GCE electrochemical electrode, indicating its excellent repeatability for quercetin detection. Furthermore, we investigated the stability of the Pt/GCE electrode over an extended period. As shown in Figure 4d, even after being exposed to air for 3 weeks, the electrode maintains 93% of its original current, demonstrating its outstanding long-term stability. Additionally, we prepared eight independent Pt/GCE electrodes under the same conditions to examine their reproducibility for quercetin detection (Figure S5, Supporting Information). Consequently, an RSD of 0.38% was achieved, indicating the excellent reproducibility of the Pt/GCE electrode for quercetin determination.

To evaluate the practical usefulness of the Pt/GCE electrode in peach vinegars, we tested its detection capability in three distinct types of peach vinegar samples obtained from a local supermarket in China, which were labeled A (from Shanxi Province), B (from Sichuan Province), and C (from Guangxi Province). The supernatant from each sample was collected by centrifugation and subsequently diluted 1000-fold using a Britton−Robinson solution (pH: 2.0). Figure S6 in the Supporting Information shows that the electrode produced steady DPV signals when detecting quercetin in various peach vinegar samples. Table 2 displays the statistical data of the quercetin concentration identified in vinegars with varying quantities of quercetin added. The findings demonstrated that quercetin is widely present in peach vinegar, and its content is extremely low (1.62−1.93 nM). Nonetheless, the Pt/GCE electrode can accurately detect quercetin selectively, with recoveries ranging from 99.5 to 101.8%. To ensure precision in our testing, we performed five repeated experiments on each sample. As a result, the RSD obtained from each repeat experiment was relatively low (1.4 to 2.3%).

Table 2. Statistic Detection Performance of the Pt/GCE Electrode in Peach Vinegars (Number = 5)

sample	added (nM)	found (nM)	recovery (%)	RSD (%)
peach vinegar A	0	1.84		1.8
	60	61.53	99.5	1.4
	120	122.11	100.2	1.7
peach vinegar B	0	1.93		2.1
	60	61.32	99.1	2.1
	120	121.18	99.3	1.9
peach vinegar C	0	1.62		2.2
	60	62.73	101.8	1.8
	120	122.85	101.0	2.3

4. CONCLUSIONS

In summary, this review presents a detailed analysis of the morphology and crystal structure of Pt nanocrystals, which were found to have a uniform hexagonal shape with an average size of 8−10 nm. The electrochemical properties of quercetin on Pt/GCE electrodes had been investigated using DPV response curves, and it was found that the Pt/GCE electrode exhibited strong electrocatalytic effects toward quercetin. The impedance properties showed that the electron-transfer process could be facilitated significantly in the Pt/GCE electrode. The effects of accumulation time, potential, and pH on the DPV response for quercetin on the Pt/GCE electrode were investigated, and optimal conditions were identified. As a result, a high sensitivity of 58 μA μM^{-1} in solutions was achieved. The Pt/GCE electrode also demonstrated outstanding selectivity, repeatability, long-term stability, and reproducibility. In the end, three distinct samples of peach vinegar were examined by using the Pt/GCE electrode, showcasing its practical efficacy in real-world implementations involving peach vinegar. Overall, the findings of this study may have important implications for the development of more efficient and sensitive electrochemical sensors for the detection of quercetin and other analytes.

■ ASSOCIATED CONTENT

Supporting Information

The Supporting Information can be addressed in Supporting Information The Supporting Information is available free of charge at https://pubs.acs.org/doi/10.1021/acsomega.3c08513.

Methods and measurements, size statistics of Pt nanocrystals, CV curves of the quercetin on electrodes, peak currents of DPV responses of accumulation time, and DPV responses of the quercetin on the Pt/GCE electrode in peach vinegar (PDF)

https://doi.org/10.1021/acsomega.3c08513
ACS Omega 2024, 9, 1850−1857

AUTHOR INFORMATION

Corresponding Authors

Xilin Peng − *School of Food and Chemical Engineering, Shaoyang University, Shaoyang 422000, P. R. China*; Email: 241848984@qq.com

Feng Gao − *School of Food and Chemical Engineering, Shaoyang University, Shaoyang 422000, P. R. China*; orcid.org/0000-0001-5273-7627; Email: gaofeng137@tju.edu.cn

Author

Ying Zhang − *School of Food and Chemical Engineering, Shaoyang University, Shaoyang 422000, P. R. China*

Complete contact information is available at: https://pubs.acs.org/10.1021/acsomega.3c08513

Notes

The authors declare no competing financial interest.

ACKNOWLEDGMENTS

The authors thank the Natural Science Foundation of Hunan Province (grant no.: 2019JJ50558) and the Foundation of Postgraduate Innovation Project (funding source: CX2022SY082) for financial support.

REFERENCES

(1) Budak, N. H.; Aykin, E.; Seydim, A. C.; Greene, A. K.; Guzel-Seydim, Z. B. Functional properties of vinegar. *J. Food Sci.* **2014**, *79*, R757−R764.

(2) Ousaaid, D.; Mechchate, H.; Laaroussi, H.; Hano, C.; Bakour, M.; El Ghouizi, A.; Conte, R.; Lyoussi, B.; El Arabi, I. Fruits Vinegar: Quality Characteristics, Phytochemistry, and Functionality. *Molecules* **2021**, *27*, 222.

(3) Kandylis, P.; Bekatorou, A.; Dimitrellou, D.; Plioni, I.; Giannopoulou, K. Health Promoting Properties of Cereal Vinegars. *Foods* **2021**, *10*, 344.

(4) Theobald, A.; Müller, A.; Anklam, E. Determination of 5-Hydroxymethylfurfural in Vinegar Samples by HPLC. *J. Agric. Food Chem.* **1998**, *46*, 1850−1854.

(5) Cavdaroglu, C.; Ozen, B. Detection of vinegar adulteration with spirit vinegar and acetic acid using UV-visible and Fourier transform infrared spectroscopy. *Food Chem.* **2022**, *379*, 132150.

(6) Fuentes, J.; Atala, E.; Pastene, E.; Carrasco-Pozo, C.; Speisky, H. Quercetin Oxidation Paradoxically Enhances its Antioxidant and Cytoprotective Properties. *J. Agric. Food Chem.* **2017**, *65*, 11002−11010.

(7) Qi, W.; Qi, W.; Xiong, D.; Long, M. Quercetin: Its Antioxidant Mechanism, Antibacterial Properties and Potential Application in Prevention and Control of Toxipathy. *Molecules* **2022**, *27*, 6545.

(8) Atala, E.; Fuentes, J.; Wehrhahn, M. J.; Speisky, H. Quercetin and related flavonoids conserve their antioxidant properties despite undergoing chemical or enzymatic oxidation. *Food Chem.* **2017**, *234*, 479−485.

(9) Dwiecki, K.; Kwiatkowska, P.; Siger, A.; Staniek, H.; Nogala-Kałucka, M.; Polewski, K. Determination of quercetin in onion (<scp>A</scp>llium *cepa*) using *β*-cyclodextrin-coated CdSe/ZnS quantum dot-based fluorescence spectroscopic technique. *Int. J. Food Sci. Technol.* **2015**, *50*, 1366−1373.

(10) Baranowska, I.; Raróg, D. Application of derivative spectrophotometry to determination of flavonoid mixtures. *Talanta* **2001**, *55*, 209−212.

(11) Ravichandran, R.; Rajendran, M.; Devapiriam, D. Antioxidant study of quercetin and their metal complex and determination of stability constant by spectrophotometry method. *Food Chem.* **2014**, *146*, 472−478.

(12) Li, Y.-Y.; Zhang, Q.-F.; Sun, H.; Cheung, N.-K.; Cheung, H.-Y. Simultaneous determination of flavonoid analogs in Scutellariae Barbatae Herba by *β*-cyclodextrin and acetonitrile modified capillary zone electrophoresis. *Talanta* **2013**, *105*, 393−402.

(13) Memon, A. F.; Solangi, A. R.; Memon, S. Q.; Mallah, A.; Memon, N.; Memon, A. A. Simultaneous Determination of Quercetin, Rutin, Naringin, and Naringenin in Different Fruits by Capillary Zone Electrophoresis. *Food Anal. Methods* **2017**, *10*, 83−91.

(14) Gencoglu, A.; Minerick, A. R. Electrochemical detection techniques in micro- and nanofluidic devices. *Microfluid. Nanofluidics* **2014**, *17*, 781−807.

(15) Bansod, B.; Kumar, T.; Thakur, R.; Rana, S.; Singh, I. A review on various electrochemical techniques for heavy metal ions detection with different sensing platforms. *Biosens. Bioelectron.* **2017**, *94*, 443−455.

(16) Gao, F.; Hong, W.; Xu, B.; Wang, Y.; Lu, L.; Zhao, Z.; Zhang, C.; Deng, X.; Tang, J. MXene Nanosheets Decorated with Pt Nanostructures for the Selective Electrochemical Detection of Quercetin. *ACS Appl. Nano Mater.* **2023**, *6*, 6869−6878.

(17) Sun, Y.; Wang, B.; He, X.; Wang, Y.; Chen, L.; Zhu, Y.; Li, G.; Sun, W. Fabrication of a $Ti_3C_2T_x$ modified glassy carbon electrode for the sensitive electrochemical detection of quercetin. *New J. Chem.* **2021**, *45*, 20396−20401.

(18) Mei, L.; Shi, Y.; Shi, Y.; Yan, P.; Lin, C.; Sun, Y.; Wei, B.; Li, J. Multivalent SnO_2 quantum dot-decorated Ti_3C_2 MXene for highly sensitive electrochemical detection of Sudan I in food. *Analyst* **2022**, *147*, 5557−5563.

(19) Zheng, J.; Wang, B.; Ding, A.; Weng, B.; Chen, J. Synthesis of MXene/DNA/Pd/Pt nanocomposite for sensitive detection of dopamine. *J. Electroanal. Chem.* **2018**, *816*, 189−194.

(20) Liu, C.; Huang, J.; Wang, L. Electrochemical synthesis of a nanocomposite consisting of carboxy-modified multi-walled carbon nanotubes, polythionine and platinum nanoparticles for simultaneous voltammetric determination of myricetin and rutin. *Microchim. Acta* **2018**, *185*, 414.

(21) Khand, N. H.; Solangi, A. R.; Ameen, S.; Fatima, A.; Buledi, J. A.; Mallah, A.; Memon, S. Q.; Sen, F.; Karimi, F.; Orooji, Y. A new electrochemical method for the detection of quercetin in onion, honey and green tea using Co_3O_4 modified GCE. *J. Food Meas. Char.* **2021**, *15*, 3720−3730.

(22) Zhao, P.; Ni, M.; Xu, Y.; Wang, C.; Chen, C.; Zhang, X.; Li, C.; Xie, Y.; Fei, J. A novel ultrasensitive electrochemical quercetin sensor based on MoS_2-carbon nanotube @ graphene oxide nanoribbons/HS-cyclodextrin/graphene quantum dots composite film. *Sens. Actuators, B* **2019**, *299*, 126997.

(23) Zhou, Z.; Gu, C.; Chen, C.; Zhao, P.; Xie, Y.; Fei, J. An ultrasensitive electrochemical sensor for quercetin based on 1-pyrenebutyrate functionalized reduced oxide graphene/mercapto-*β*-cyclodextrin/Au nanoparticles composite film. *Sens. Actuators, B* **2019**, *288*, 88−95.

(24) Qiu, X.; Lu, L.; Leng, J.; Yu, Y.; Wang, W.; Jiang, M.; Bai, L. An enhanced electrochemical platform based on graphene oxide and multi-walled carbon nanotubes nanocomposite for sensitive determination of Sunset Yellow and Tartrazine. *Food Chem.* **2016**, *190*, 889−895.

(25) Wang, Y.; Wang, J.; Han, G.; Du, C.; Deng, Q.; Gao, Y.; Yin, G.; Song, Y. Pt decorated Ti_3C_2 MXene for enhanced methanol oxidation reaction. *Ceram. Int.* **2019**, *45*, 2411−2417.

(26) Lorencova, L.; Bertok, T.; Filip, J.; Jerigova, M.; Velic, D.; Kasak, P.; Mahmoud, K. A.; Tkac, J. Highly stable Ti_3C_2Tx (MXene)/Pt nanoparticles-modified glassy carbon electrode for H_2O_2 and small molecules sensing applications. *Sens. Actuators, B* **2018**, *263*, 360−368.

(27) Li, B.; Ye, R.; Wang, Q.; Liu, X.; Fang, P.; Hu, J. Facile synthesis of coral-like Pt nanoparticles/MXene (Ti_3C_2Tx) with efficient hydrogen evolution reaction activity. *Ionics* **2021**, *27*, 1221−1231.

(28) Shi, Y.; Liu, Z.; Liu, R.; Wu, R.; Zhang, J. DNA-encoded MXene-Pt nanozyme for enhanced colorimetric sensing of mercury ions. *Chem. Eng. J.* **2022**, *442*, 136072.
(29) An, K.; Musselwhite, N.; Kennedy, G.; Pushkarev, V. V.; Robert Baker, L.; Somorjai, G. A. Preparation of mesoporous oxides and their support effects on Pt nanoparticle catalysts in catalytic hydrogenation of furfural. *J. Colloid Interface Sci.* **2013**, *392*, 122−128.
(30) Manokaran, J.; Muruganantham, R.; Muthukrishnaraj, A.; Balasubramanian, N. Platinum-polydopamine @SiO_2 nanocomposite modified electrode for the electrochemical determination of quercetin. *Electrochim. Acta* **2015**, *168*, 16−24.
(31) Deng, X.; Yin, S.; Xie, Z.; Gao, F.; Jiang, S.; Zhou, X. Synthesis of silver@platinum-cobalt nanoflower on reduced graphene oxide as an efficient catalyst for oxygen reduction reaction. *Int. J. Hydrogen Energy* **2021**, *46*, 17731−17740.
(32) Xia, T.; Liu, G.; Wang, J.; Hou, S.; Hou, S. MXene-based enzymatic sensor for highly sensitive and selective detection of cholesterol. *Biosens. Bioelectron.* **2021**, *183*, 113243.
(33) Zare, H. R.; Namazian, M.; Nasirizadeh, N. Electrochemical behavior of quercetin: Experimental and theoretical studies. *J. Electroanal. Chem.* **2005**, *584*, 77−83.
(34) Wang, Q.; Zhou, H.; Hao, T.; Hu, K.; Qin, L.; Ren, X.; Guo, Z.; Wang, S.; Hu, Y. A fully integrated fast scan cyclic voltammetry electrochemical method: Improvements in reaction kinetics and signal stability for specific Ag(I) and Hg(II) analysis. *J. Electroanal. Chem.* **2022**, *910*, 116208.
(35) Xu, B.; Yang, L.; Zhao, F.; Zeng, B. A novel electrochemical quercetin sensor based on Pd/MoS_2-ionic liquid functionalized ordered mesoporous carbon. *Electrochim. Acta* **2017**, *247*, 657−665.
(36) Sabbaghi, N.; Azizi-Khereshki, N.; Farsadrooh, M.; Elyasi, Z.; Javadian, H.; Sadeghi, M.; Shafiee-Kisomi, A. Synthesis of poly-(dopamine quinone-chromium(III) complex) @hierarchical cabbage flower-like cobalt as a novel mesoporous nanocomposite modifier of graphite paste electrode for electrochemical determination of quercetin in biological samples. *Colloids Surf., A* **2022**, *643*, 128739.
(37) Veerakumar, P.; Rajkumar, C.; Chen, S.-M.; Thirumalraj, B.; Lin, K.-C. Ultrathin 2D graphitic carbon nitride nanosheets decorated with silver nanoparticles for electrochemical sensing of quercetin. *J. Electroanal. Chem.* **2018**, *826*, 207−216.
(38) Kan, X.; Zhang, T.; Zhong, M.; Lu, X. CD/AuNPs/MWCNTs based electrochemical sensor for quercetin dual-signal detection. *Biosens. Bioelectron.* **2016**, *77*, 638−643.
(39) Karuppasamy, P.; Karthika, A.; Senthilkumar, S.; Rajapandian, V. An Efficient and Highly Sensitive Amperometric Quercetin Sensor Based on a Lotus Flower Like SeO_2-Decorated rGO Nanocomposite Modified Glassy Carbon Electrode. *Electrocatalysis* **2022**, *13*, 269−282.

https://doi.org/10.1021/acsomega.3c08513
ACS Omega 2024, 9, 1850−1857